ELSEVIER

Contents lists available at ScienceDirect

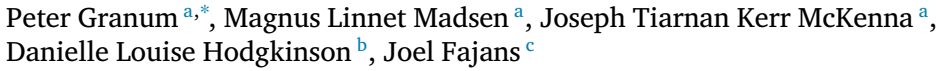
# Nuclear Inst. and Methods in Physics Research, A

journal homepage: www.elsevier.com/locate/nima



# **Technical Notes**

# Efficient calculations of magnetic fields of solenoids for simulations



- <sup>a</sup> Department of Physics and Astronomy, Aarhus University, Aarhus, Denmark
- <sup>b</sup> School of Physics and Astronomy, University of Manchester, Manchester, UK
- <sup>c</sup> Department of Physics, University of California at Berkeley, Berkeley, CA, USA



# ARTICLE INFO

#### Keywords: Magnets Solenoids Simulations Magnetic fields Efficiency Field models

#### ABSTRACT

This paper examines different models for calculating the magnetic field of solenoids. Accuracy and computation time are compared for a range of different simplified models: a current loop and a thin shell solenoid, and solenoids with finite length and thickness. There is no definitive answer to "what model is the best", as it depends on the specific use case, but there are certain models that excel in speed or accuracy, and there are models that have very limited use. This paper serves as an overview and will help the reader make an informed choice of a model.

#### 1. Introduction

Simulating the behaviour of trapped particles often requires the calculation of magnetic fields. Even if exact analytic expressions are available for the given magnet configuration, they are often slow to compute. Simulations often involve high numbers of particles, whose behaviour have to be evaluated over many time steps, so one must often make a compromise between computation time and accuracy. This paper evaluates these parameters for a range of methods.

This study was done in the context of the ALPHA experiment at CERN, which measures the properties of antihydrogen to test CPT symmetry by comparison with hydrogen. The antihydrogen is produced by mixing positron and antiproton plasmas confined by Penning–Malmberg traps, and the electrically neutral antihydrogen atoms are confined via their magnetic moment in a magnetic (Ioffe–Pritchard) trap. A description of the experiment and a selection of results can be found in [1–10]. Besides the existing ALPHA-2 atom trap, a more complicated atom trap called ALPHA-g is under construction. The purpose of ALPHA-g is to measure how antihydrogen behaves in Earth's gravitational field to test the Weak Equivalence Principle, which requires control of the magnetic field to the 1 to 10 ppm level. It has previously been demonstrated that the field can be measured to such precision [11].

Most of the magnets in ALPHA are relatively short solenoids, but this paper will focus on solenoids without any assumptions about their length to radius ratio. The model used to represent the physical geometry of a magnet will be referred to as a *magnet model*, and the model used to calculate the magnetic field will be referred to as a *field*  *model.* For each field model, we calculate the magnetic field along the four paths illustrated in Fig. 1, and present its accuracy. The coordinate system is centred at the geometrical centre of the solenoid, which has radius R. The four paths are referred to as  $\rho$  on (1),  $\rho$  off (2), z on (3), and z off (4). The z on path coincides with the symmetry axis of the solenoid (the z-axis), and the z off path is perpendicular to the z-axis but offset by R/2 in the x-direction P1. The P2 on path lies in the centre plane of the solenoid, and the P2 off path is displaced by P3 in the P3-direction.

To aid in the choice of a model, the accuracy and computation time for the different models will be presented. The code used to calculate the field of the different models is available on Github: <a href="https://github.com/pgranum/BFieldModels\_Public">https://github.com/pgranum/BFieldModels\_Public</a>. A list of the different models examined in this paper can be seen in Table 1.

# 2. Field model accuracy

To evaluate the accuracy of field models for a magnet model, there must be a *reference model* that is considered to give the *true* value of the field,  $B_{ref}$ . For the simpler magnet models, exact analytic expressions are available. For more complicated magnet models, a detailed Biot–Savart model can be used. As the *accuracy* metric of the field B of a given model, we will use

$$\Delta B/B_0 \equiv \frac{B(x, y, z) - B_{\text{ref}}(x, y, z)}{B_{\text{ref}}(0, 0, 0)}$$
 (1)

This metric emphasizes the field in the central region of the magnet. In configurations with multiple magnets, like particle traps, the central

<sup>\*</sup> Corresponding author.

E-mail address: peter.granum@cern.ch (P. Granum).

<sup>&</sup>lt;sup>1</sup> As the geometry of the solenoid in theory is azimuthally symmetric, the direction of the offset is irrelevant.

Table 1

A list of the different models and their qualitative characteristics. \*For several of the models the accuracy and computation time depend on a variable parameter. The ratings given here are based on a crude estimate of the instances of the models studied in this paper.

Model type/name	Abbreviation	Reference model [yes/no]	Qualitative accuracy*	Qualitative computation time*
Circular Current Loop				
Simple Analytic Model	SAM	yes	exact	average
McDonald	McD	no	good	good
Biot-Savart		no	good	bad
Jackson		no	poor	-
Numerical Integration of Infinite Integrals		no	-	very poor
Thin Shell Solenoid				
Conway		yes	exact	average
McDonald	McD	no	good	good
N-Wire		no	average	poor
Gaussian Quadrature with Loops	GQ	no	good	average
Finite Solenoids				
Biot-Savart		yes	exact	very poor
Truncated Approximate Vector Potential	TAVP	no	very poor	good
McDonald	McD	no	good	average
N-Wire		no	good	poor
Gaussian Quadrature with Loops	GQ	no	average	average
Gaussian Quadrature with Shells	GQ	no	good	average

region is where the solenoid's contribution to the total magnetic field is the most significant. For example, if the solenoid is immersed in an external magnetic field, the contribution of the solenoid's field to the total field will be small far from the solenoid's centre.

We base our magnet models on one of the superconducting solenoids in the ALPHA-2 experiment. The solenoid has inner and outer radius  $R_1=41.25~\mathrm{mm}$  and  $R_2=46.37~\mathrm{mm}$ , length  $L=34.68~\mathrm{mm}$ , 4 layers with 30 windings per layer, layer spacing  $\Delta\rho=1.707~\mathrm{mm}$ , and spacing between wires in a given layer  $\Delta z=1.196~\mathrm{mm}$ . The current running though the magnet is  $I=600~\mathrm{A}$ . In this paper, lengths will be normalised to the radius of the magnet, and magnetic fields to the field at the centre of the magnet. Although the simulations in this paper will be based on our magnet, the results are expected to be true for other magnets.

# 3. Computation time

The field models are implemented in C++ in a similar style, which allows rough comparisons of the computation time. The models have been written without architecture targeted optimisations, as extreme optimisation is not in the scope of this paper. The computation time of each method was measured using the class steady\_clock from the standard library std::chrono.

We measure a models' computation time as the time it takes for a model to be executed at 100 equidistant points along each of the four paths seen in Fig. 1. The computation time is independent of the position within a factor of 3. Fig. 2 shows the computation time as a function of position for the Conway model (see Section 5.1), a model with a large variance in computation time. This variance is likely an artefact of the CPU's branch prediction, as the algorithm of the Conway model contains the largest number of "if" statements. At each position, the field is calculated 10000 times. A histogram of the resulting one million calculations is seen in Fig. 3. The histogram qualitatively represents of all the field models. In theory the calculation is deterministic, so any difference in computation time for the same position is due to a varying load on the CPU. The histogram shows that there is a minimum computation time. Most computation times lie just above the cutoff.

To determine the computation time for a given position, we use the median of the 10000 different computation times. Since the median is the same within a factor of 3 across all 100 positions, we use the median of the 100 median computation times as the computation time for a given path. Hence, a total of  $10000 \cdot 100 = 10^6$  calculations go into the determination of the computation time for a given path. The computation time has proven to be roughly path independent, within

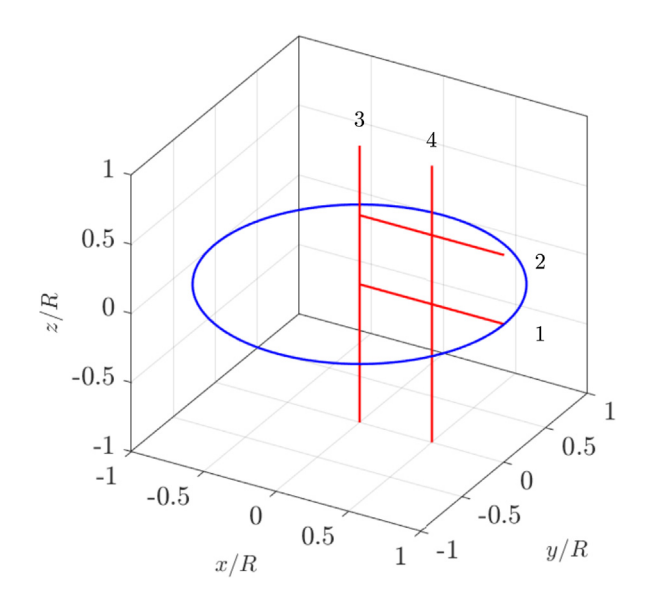


Fig. 1. A sketch of solenoid represented by a current loop (blue) with radius R placed in the x-y-plane and four paths (red) numbered 1 to 4 ( $\rho$  on,  $\rho$  off, z on, and z off). It is along these paths that the magnetic field of the different models has been calculated and compared.

a factor of 3, so we chose the *z off* path to be representative for every model. For the Conway model used in Figs. 2 and 3, the computation time is 2.0  $\mu s$ . Even though the computation time is only precise to an order of magnitude, we give two significant digits to allow comparisons of different models. Note that the computation time depends on the particular computer system.

All quoted processing times are based on a Intel Core i5-8600K with 16 GB of Dual Channel Corsair Vengeance LPX DDR4 memory running at 3000MHz. Warm up calculations were used to make sure the system was thermally stable for all measurements.

#### 4. Circular current loop

A circular current loop is a time-independent current moving in a circle with a fixed radius. A sketch of a circular current loop with radius R placed in a cylindrical coordinate system  $(\rho, \phi, z)$  centred around the z-axis is seen in Fig. 4. The on-axis field of a current loop with radius

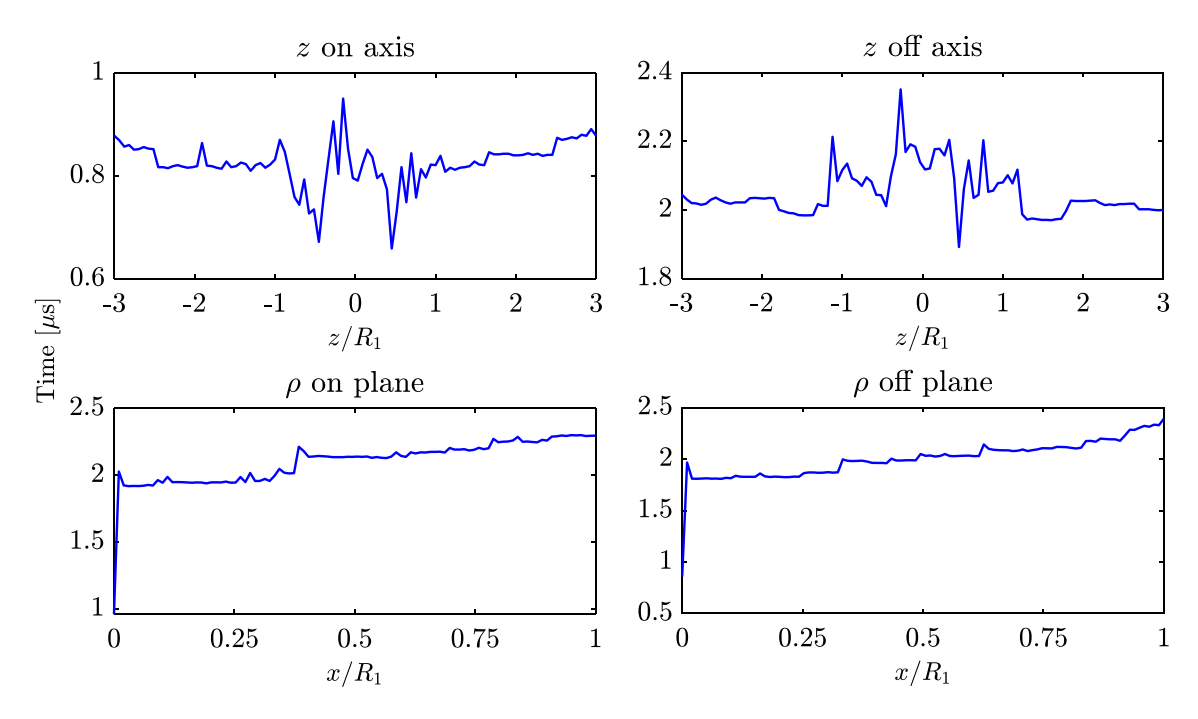


Fig. 2. The computation time as a function of position along the four different paths for the Conway model. Relative to the other models, the computation time for this model fluctuates significantly as a function of position.

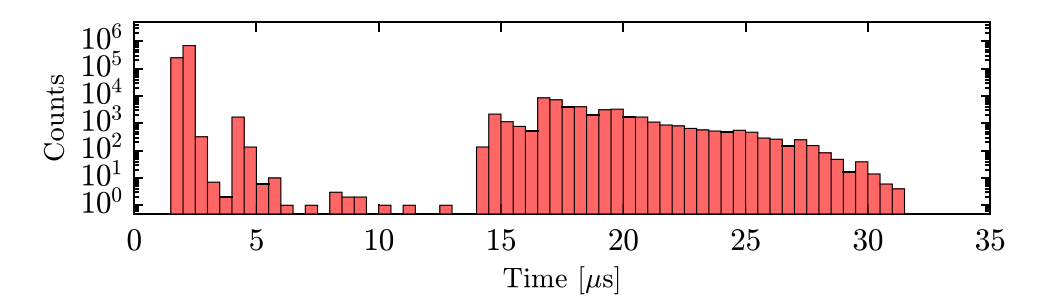


Fig. 3. A histogram of the calculation time along path 4 (z off) of a Conway model. The model has been executed 1 million times. The computation times have been combined into bins of width  $0.5~\mu s$  and plotted on a logarithmic scale.

R and current I (see Griffiths' [12]) is given as

$$B_z(0,0,z) = \frac{\mu_0 I}{2} \frac{R^2}{(R^2 + z^2)^{3/2}} \tag{2}$$

where  $\mu_0$  is the vacuum permeability. The radius of a current loop is calculated as the average of the inner and outer radius of our magnet (43.81 mm). The current in the single loop is the same as the current in the magnet multiplied by the number of windings (72000 A).

# 4.1. Simple analytic model

The Simple Analytic Model (SAM), derived for example by James Simpson et al. [13], provides an exact analytical expression for the magnetic field of a circular current. Simpson et al. derived multiple exact expressions for the magnetic field and vector potential of a current loop in different coordinate systems. In cylindrical coordinates  $(\rho, \phi, z)$  the expression for the magnetic field is

$$B_{\rho} = \frac{Cz}{2\alpha^{2}\beta\rho} \left[ (R^{2} + \rho^{2} + z^{2})E(k^{2}) - \alpha^{2}K(k^{2}) \right], \tag{3}$$

$$B_{\phi} = 0, \tag{4}$$

$$B_z = \frac{C}{2\alpha^2 \beta} \left[ (R^2 - \rho^2 + z^2) E(k^2) + \alpha^2 K(k^2) \right], \tag{5}$$

where

$$\alpha^2 = R^2 + \rho^2 + z^2 - 2R\rho, (6)$$

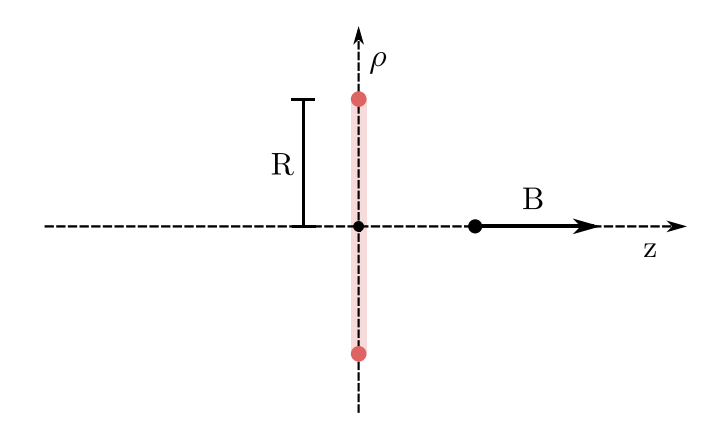


**Fig. 4.** A sketch of a circular current loop with radius R in a cylindrical coordinate system centred around the z-axis. The current distribution creates a magnetic field on the axis pointing in the z-direction.

$$\beta^2 = R^2 + \rho^2 + z^2 + 2R\rho,\tag{7}$$

$$k^2 = 1 - \frac{\alpha^2}{\beta^2},\tag{8}$$

$$C = \frac{\mu_0 I}{}.$$
 (9)

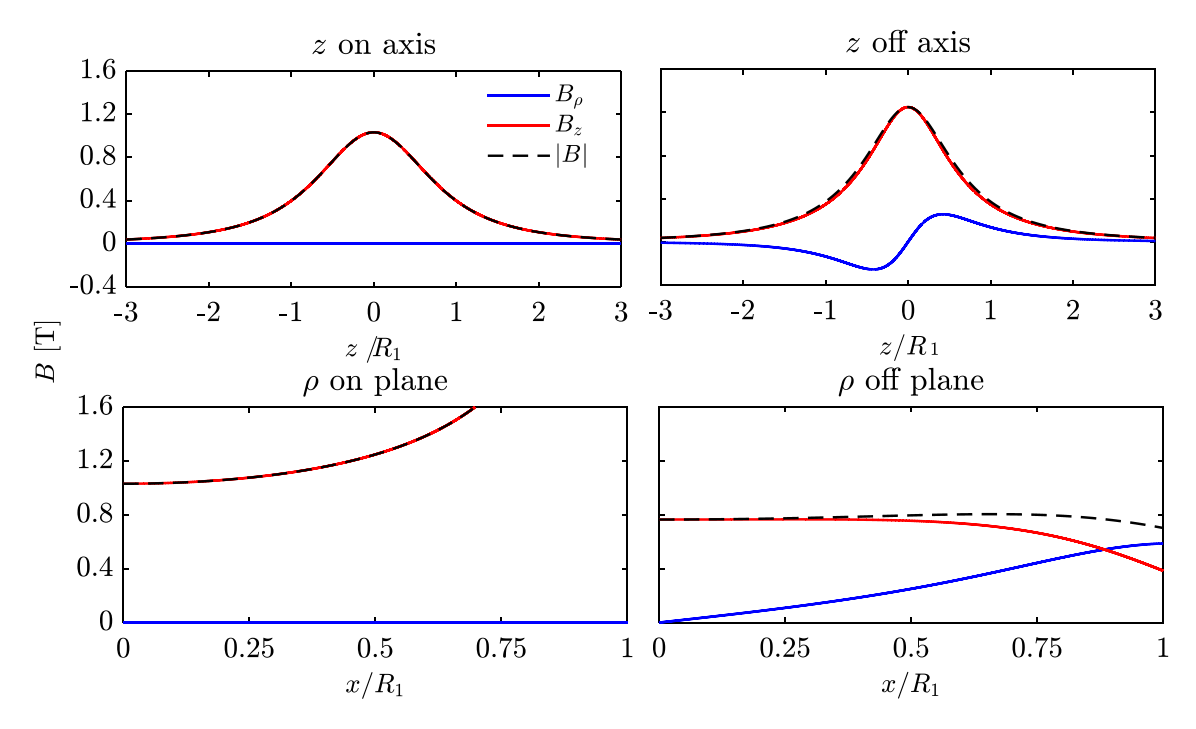


Fig. 5. The magnitude and  $\rho$  and z components of the magnetic field generated by a current loop with radius R = 43.81 mm and current I = 72000 A as calculated by the SAM model along the four paths shown in Fig. 1. The azimuthal component,  $B_{ab}$ , is always zero.

K(x) and E(x) are the complete elliptic integrals of the first and second kind available in the <cmath> package in C++ using the functions comp\_ellint\_1 and comp\_ellint\_2. Notice that the functions in <cmath> take k rather than  $k^2$  as an argument. Both conventions are common in the literature. The resulting magnetic field along the four paths is seen in Fig. 5. This field model will be used throughout this chapter as a reference model  $B_{ref}(x, y, z)$ .

#### 4.2. McDonald model

Kirk T. McDonald [14] has derived a series expansion for the off-axis field of an azimuthally symmetric magnetic field based on its axial field  $B_z(0,0,z)$ . We will refer to this as the McDonald model. The expression for the McDonald model is exact on the axis but only approximate off-axis. The components of the magnetic field are given by

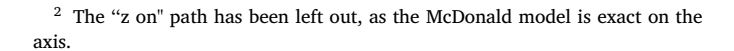
$$B_z(\rho, z) = \sum_{n=0} (-1)^n \frac{a_0^{(2n)}(z)}{(n!)^2} \left(\frac{\rho}{2}\right)^{2n}$$
 (10)

$$B_{\rho}(\rho, z) = \sum_{n=0}^{\infty} (-1)^{n+1} \frac{a_0^{(2n+1)}(z)}{(n+1)(n!)^2} \left(\frac{\rho}{2}\right)^{2n+1}$$
(11)

where

$$a_0^{(n)} = \frac{d^n a_0}{dz^n}$$
 and  $a_0(z) = B_z(0, 0, z)$  (12)

Together with the axial-field of a current loop given by Eq. (2), the field can be approximated at any point in space. The expansion has been tested up to 7th order, and the accuracy of the different orders along the paths z of  $f^2$  and  $\rho$  on/of can be seen in Figs. 6 and 7. To see the accuracy of the higher order, all plots have a zoomed-in version below them. Unsurprisingly the accuracy of the model increases with the order.



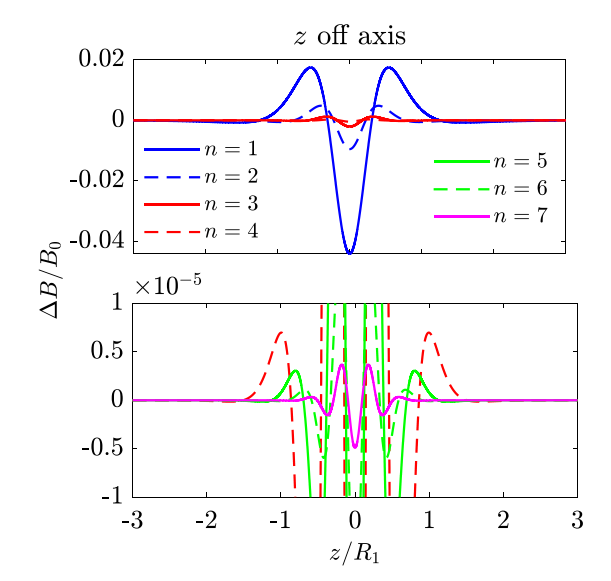


**Fig. 6.** The accuracy of the McDonald model along path z off. The upper plot displays the orders 1-4 while the lower plot is zoomed in on the  $\Delta B/B_0$  axis displays the orders  $\frac{1}{2}$ 

# 4.3. Biot-Savart model

Another way of calculating the magnetic field of a current loop is to approximate the loop as consisting of N straight line segments with equal lengths and adding their individual field contributions together to get the total magnetic field. Consider a small line segment of a closed current loop of length  $d\mathbf{l}$  pointing in the direction of the current flow. A current I flows through the loop. The Biot–Savart law states that the line segment's contribution to the total magnetic field at an observation point P is

$$d\mathbf{B} = \frac{\mu_0 I}{4\pi} \frac{d\mathbf{l} \times \mathbf{r}}{|\mathbf{r}|^3} \tag{13}$$

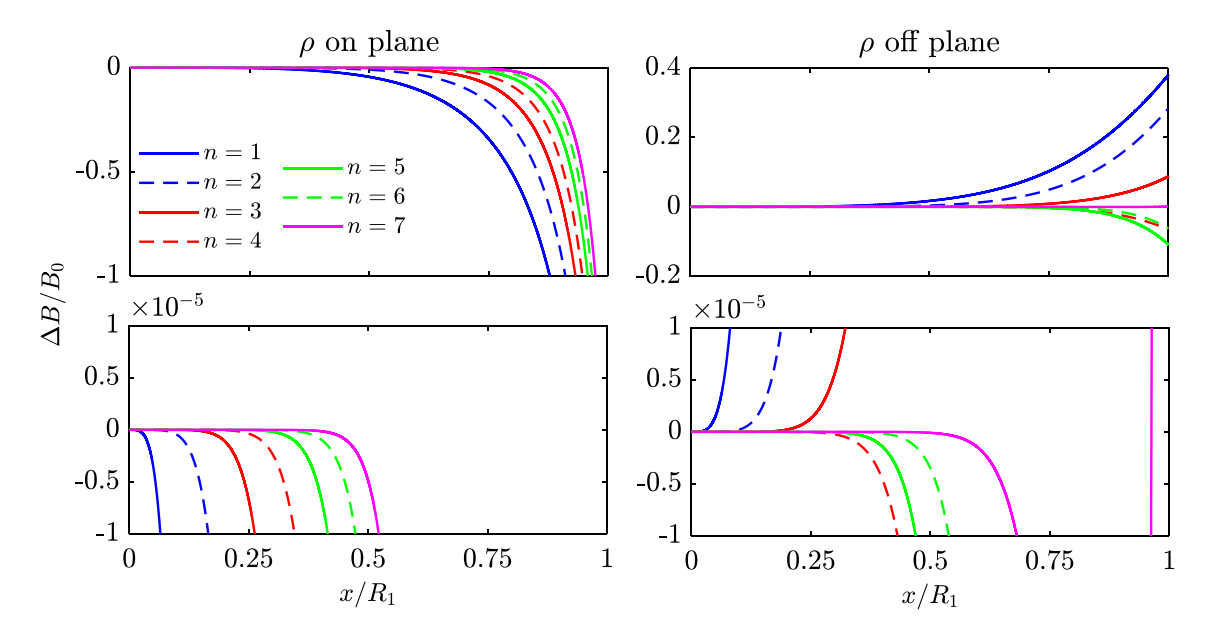


Fig. 7. The accuracy of the McDonald model along path  $\rho$  on and  $\rho$  off. The lower plots display the same data as the upper plots, but zoomed in on the  $\Delta B/B_0$  axis.

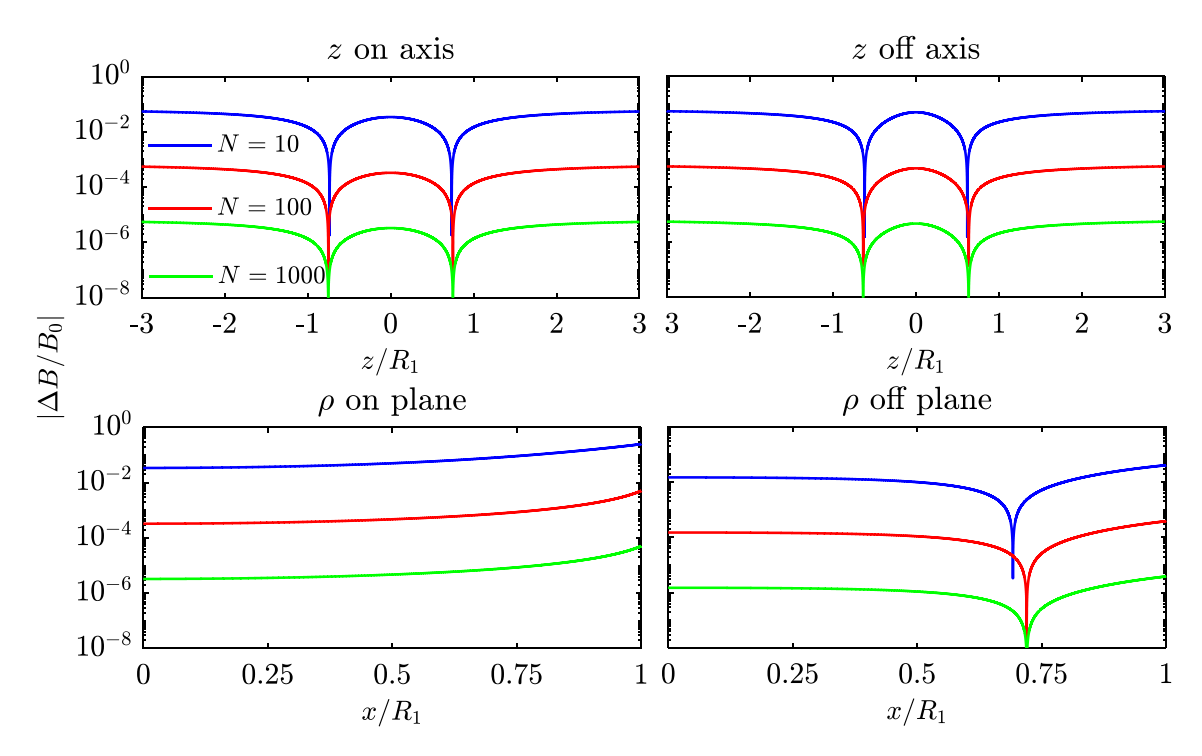


Fig. 8. The accuracy of the Biot-Savart model along the four paths, where the loop has been approximated with 10, 100 and 1000 line segments respectively.

where  $\mathbf{r}$  is the coordinate vector from the line segment to the point P. The Biot–Savart model can be used to model any magnet configuration. Within machine precision, the accuracy can be made arbitrarily small by increasing the number of line segments to better approximate the shape of the loop, but this comes at the expense of a linear increase in the computation time.

The accuracy of the Biot–Savart model along all four paths for 10, 100 and 1000 segments can be seen in Fig. 8. As the plot is logarithmic, the *absolute* value of Eq. (1) is plotted as a function of position. The sharp "dips" in the figures appear where the accuracy changes sign. As the number of line segments is increased tenfold, the accuracy of the model increases about a hundredfold. The accuracy of the 7th order

McDonald model is somewhere between the result for 100 and 1000 segments.

# 4.4. Jackson model

Assume that the magnetic field is evaluated at a point near the axis of symmetry or far away from the coil so  $R \gg r$ ,  $R \ll r$ , or  $\theta \ll 1$  in spherical coordinates  $(r,\phi,\theta)$ . The field can then be approximated as described in Jackson [15, Eq. 5.40]

$$B_r = \frac{\mu_0 I R^2 \cos \theta}{2(R^2 + r^2)^{\frac{3}{2}}} \left[ 1 + \frac{15R^2 r^2 \sin(\theta)}{4(R^2 + r^2)^2} + \cdots \right]$$
 (14)

**Table 2**The computation time for calculating the magnetic field of a current loop for the field models examined. The computation time has been determined as described in chapter 3.

described in enapter of	
Model	Time [μs]
SAM	0.34
McD loop $n = 1$	0.043
McD loop $n = 2$	0.054
McD loop $n = 3$	0.053
McD loop $n = 4$	0.061
McD loop $n = 5$	0.075
McD loop $n = 6$	0.075
McD loop $n = 7$	0.085
Biot $N = 10$	0.23
Biot $N = 100$	1.9
Biot $N = 1000$	19

$$B_{\theta} = -\frac{\mu_0 I R^2 \sin \theta}{4(R^2 + r^2)^{\frac{5}{2}}} \left[ 2R^2 - r^2 + \frac{15R^2 r^2 \sin(\theta)(4R^2 - 3r^2)}{8(R^2 + r^2)^2} + \cdots \right]$$
 (15)

Unsurprisingly the accuracy of the model is bad when the assumptions are not met. No further work went into examining the Jackson model, and the model is only mentioned here for completeness.

# 4.5. Numerical integration of infinite integrals

Another model mentioned in Jackson [15] is the expression derived in exercise 5.10,

$$B_{\rho}(\rho, z) = \frac{\mu_0 I R}{\pi} \int_0^{\infty} dk \, k \sin(kz) I_1(k\rho_{<}) K_1(k\rho_{>})$$
 (16)

$$B_z(\rho, z) = \frac{\mu_0 I R}{\pi} \int_0^\infty \mathrm{d}k \, k \cos(kz) \begin{cases} I_0(k\rho) K_1(kR) & \text{for } \rho < R \\ I_1(kR) K_0(k\rho) & \text{for } \rho > R \end{cases} \tag{17}$$

where  $K_i$  and  $I_i$  are the modified Bessel functions of the first and second kind, and  $\rho_>$  ( $\rho_<$ ) is the larger (smaller) of  $\rho$  and R. Even though the expression is in principle exact, numerical integration is required to evaluate it, which makes it non-exact. To change the integral limit from infinite to finite a change of variable can be done,

$$\int_{a}^{\infty} f(x)dx = \int_{0}^{1} f\left(a + \frac{t}{1 - t}\right) \frac{dt}{(1 - t)^{2}}$$
 (18)

but the integral does not converge. As the computation time quickly exceeds the computation time of the exact SAM model, the numerical integration model is not explored any further.

# 4.6. Discussion of loop models

The computation times for the models examined are listed in Table 2 and are determined as described in chapter 3. For the circular current loop, the McDonald approximation is seen to be faster than the SAM for the orders tested. The accuracy of the McDonald model is below  $10^{-5}$  for some of the higher order models and  $\rho/R < 0.5$ . The computation time of the Biot–Savart model is seen to exceed the computation time of the McDonald model even for a very low number of straight line segments, for which the model is not very accurate. Hence, it is a poor choice for calculating the field of a circular current loop, but it can be used for more complex current distributions. The values suggest that the computation time of the Biot–Savart model scales linearly with the number of segments.

# 5. Thin shell solenoid

A thin shell solenoid is a uniform current distribution on an infinitely thin cylindrical shell, where the current runs in the azimuthal direction. A cross sectional view of a thin shell solenoid with length L, radius R, and endpoints at  $z_1$  and  $z_2$  is seen in Fig. 9. We assume that the shell is centred around the origin, so  $z_1 = -z_2$  and  $L = 2z_1$ . The

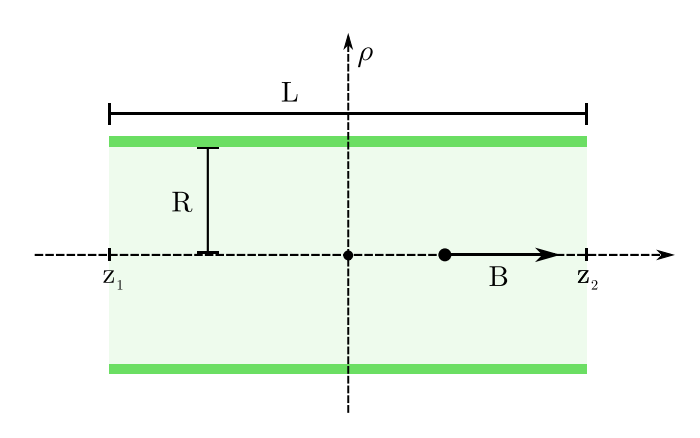


**Fig. 9.** A sketch showing a cross section of a thin shell solenoid of length L and radius R in a cylindrical coordinate system. The coordinate of the back- and front-end is denoted by  $z_1$  and  $z_2$  respectively. The current running in the azimuthal direction produces a magnetic field pointing in the z-direction on the axis.

on-axis field of the shell can be derived by integrating the equivalent expression (Eq. (2)) for a current loop over the length of the shell. Assuming that the shell consists of N current loops with a current I, the total current is IN, and the expression for the on-axis field becomes

$$B_z(0,0,z) = \frac{\mu_0 I N}{2L} \left( \frac{z - z_1}{\sqrt{R^2 + (z - z_1)^2}} - \frac{z - z_2}{\sqrt{R^2 + (z - z_2)^2}} \right)$$
(19)

Just like in chapter 4, the value used for the radius will be 43.81 mm. The current will be 600 A, the length 34.68 mm, and the number of loops, *N*, (equal to the total number of windings) will be 120.

# 5.1. Conway model

Even though the thin shell solenoid is a relatively simple current distribution, calculating the field at an arbitrary point in space is significantly harder than on the axis. An exact analytic expression for the field is derived in a paper by T. Conway [16]. This model will be referred to as the Conway model.

Let the field of a cylindrical shell be evaluated at a point in cylindrical coordinates  $(\rho, \phi, z)$ . The following parameters can then be defined

$$k = \sqrt{\frac{4\rho R}{(\rho + R)^2 + z^2}} \tag{20}$$

$$k' = \sqrt{1 - k^2} \tag{21}$$

$$\beta = \sin^{-1}\left(\frac{z}{\sqrt{(\rho - R)^2 + z^2}}\right) \tag{22}$$

Together with the complete and incomplete elliptic integral functions, Heuman's Lambda function can now be defined

$$\Lambda_0(\beta, k) = \frac{2}{\pi} \left( E(k)F(\beta, k') + K(k)E(\beta, k') - K(k)F(\beta, k') \right) \tag{23}$$

The solutions for integrals of the type

$$I_{\lambda,\mu,\nu}(R,\rho,|z|) = \int_0^\infty s^\lambda J_\mu(sR) J_\nu(s\rho) e^{-s|z|} ds \tag{24} \label{eq:24}$$

which Conway refers to as Bessel–Laplace integrals, can be expressed by the defined parameters and Heuman's Lambda function. The solutions from Conway's paper to the relevant integrals are listed here:

$$I_{0,1,0}(R,\rho,|z|) = \frac{1}{R} \left( 1 - \frac{|z|kK(k)}{2\pi\sqrt{\rho R}} - \frac{\Lambda_0(|\beta|,k)}{2} \right) \text{ for } \rho < R$$
 (25)

$$I_{0,1,0}(R,\rho,|z|) = \frac{1}{R} \left( \frac{|z|kK(k)}{2\pi\sqrt{\rho R}} + \frac{\Lambda_0(|\beta|,k)}{2} \right) \text{ for } \rho > R$$
 (26)

$$I_{0,1,1}(R,\rho,|z|) = \frac{1}{\pi k \sqrt{\rho R}} ((2 - k^2)K(k) - 2E(k))$$
 (27)

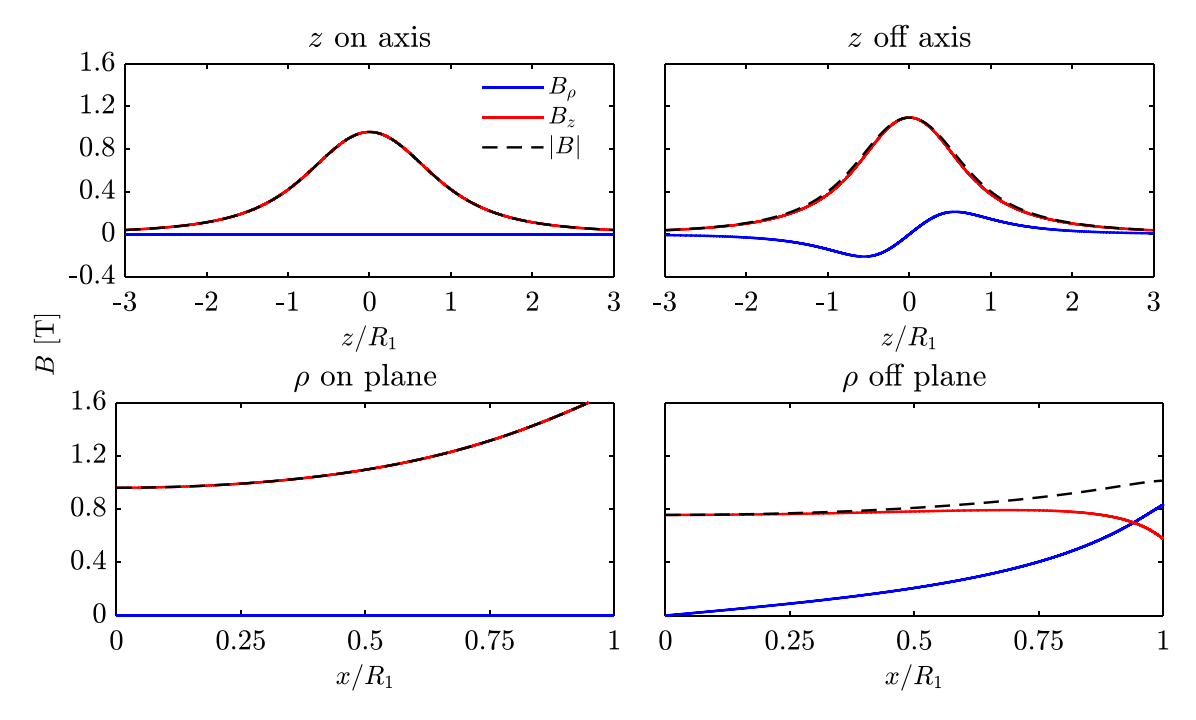


Fig. 10. The  $\rho$  and z components and the magnitude of the magnetic field generated by a thin shell solenoid with radius R = 43.81 mm, length L = 34.68 mm, current I = 600 A, and 120 windings as calculated by the Conway model along the four paths shown in Fig. 1. The azimuthal component B<sub>A</sub> is always zero and therefore omitted.

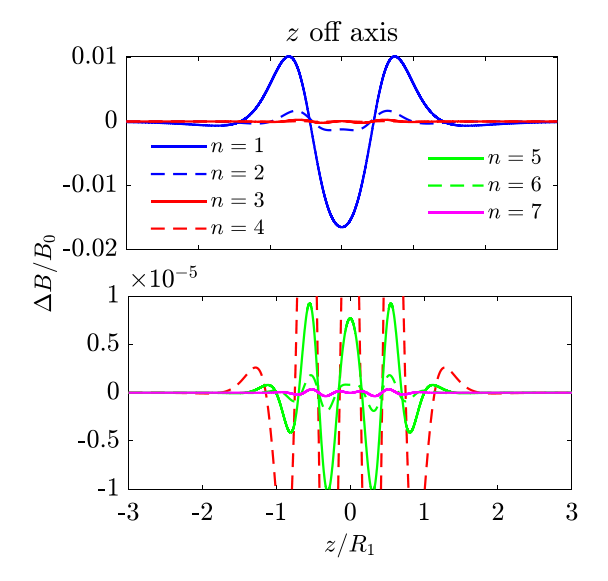


Fig. 11. The accuracy of the McDonald model along path z off. The upper plot displays the orders 1-4 while the lower plot, which is zoomed in on the  $\Delta B/B_0$  axis, displays the orders 4-7.

Analytic expressions for the magnetic field from a thin cylindrical shell of finite length are then given as

$$\begin{split} B_z &= \frac{\mu_0 I N R}{2L} \left( I_{0,1,0}(R,\rho,|z_1-z|) - I_{0,1,0}(R,\rho,|z_2-z|) \right) &\quad \text{for } z < z_1 \quad \text{(28)} \\ B_z &= \frac{\mu_0 I N R}{2L} (2 I_{0,1,0}(R,\rho,0) \\ &\quad - I_{0,1,0}(R,\rho,|z_1-z|) - I_{0,1,0}(R,\rho,|z_2-z|)) &\quad \text{for } z_1 < z < z_2 \end{split}$$

$$\begin{split} B_z &= \frac{\mu_0 I N R}{2 L} \left( I_{0,1,0}(R,\rho,|z_2-z|) - I_{0,1,0}(R,\rho,|z_1-z|) \right) &\quad \text{for } z_2 < z \qquad \text{(30)} \\ B_\rho &= \frac{\mu_0 I N R}{2 L} \left( I_{0,1,1}(R,\rho,|z_1-z|) - I_{0,1,0}(R,\rho,|z_2-z|) \right) \end{split} \label{eq:Bz}$$

$$B_{\rho} = \frac{\mu_0 I N R}{2 I_{\bullet}} \left( I_{0,1,1}(R, \rho, |z_1 - z|) - I_{0,1,0}(R, \rho, |z_2 - z|) \right)$$
 (31)

As Conway writes, these expressions are not new, but they do not seem to be included in the popular textbooks. The resulting magnetic field along all four paths are seen Fig. 10. The Conway field model will be used as a reference model for a thin cylindrical shell. Conway's paper also presents an expression for the field of a cylindrical shell with a finite thickness, but the expression for the axial component of the field is given as an integral that would have to be evaluated numerically. The expression is therefore no longer exact, and the numerical integration would be slow. Hence, the field model for a shell with finite thickness will not be considered later.

# 5.2. McDonald model

The field of a shell solenoid is naturally azimuthally symmetric. Consequently the McDonald model introduced in Section 4.2 can be applied to approximate the field of a shell solenoid at any point in space by expanding equation (19). Figs. 11 and 12 show the accuracy of different orders of the McDonald model compared to the exact Conway model from Section 5.1. There is no deviation from the exact model on axis, so the plot for the z on path has been omitted. Unsurprisingly the model is less accurate further away from the axis and more accurate at higher order.

# 5.3. N-wire model of a thin shell solenoid

A thin shell solenoid can be represented by a number of equidistant discrete circular current loops placed over the length of the shell. The number of loops, N, is chosen to match the number of windings per layer, which is 30 in the magnet used as a model. This field model will be referred to as the N-Wire model. To make the total current the same as in the Conway model used for reference, the current in each individual loop is multiplied by the number of layers to give a total of 2400 A per loop. The spacing between the circular current loops is given by  $\Delta z = \frac{L}{30}$ , meaning that the centre of the wire represented by the leftmost loop is positioned at  $z_1 + \frac{\Delta z}{2}$ . Hence, the wire extends to the edge of the shell. This is illustrated in Fig. 13. It would be incorrect to make the centre of the leftmost wire coincide with the left edge of the shell, as the loops would then represent the same amount of

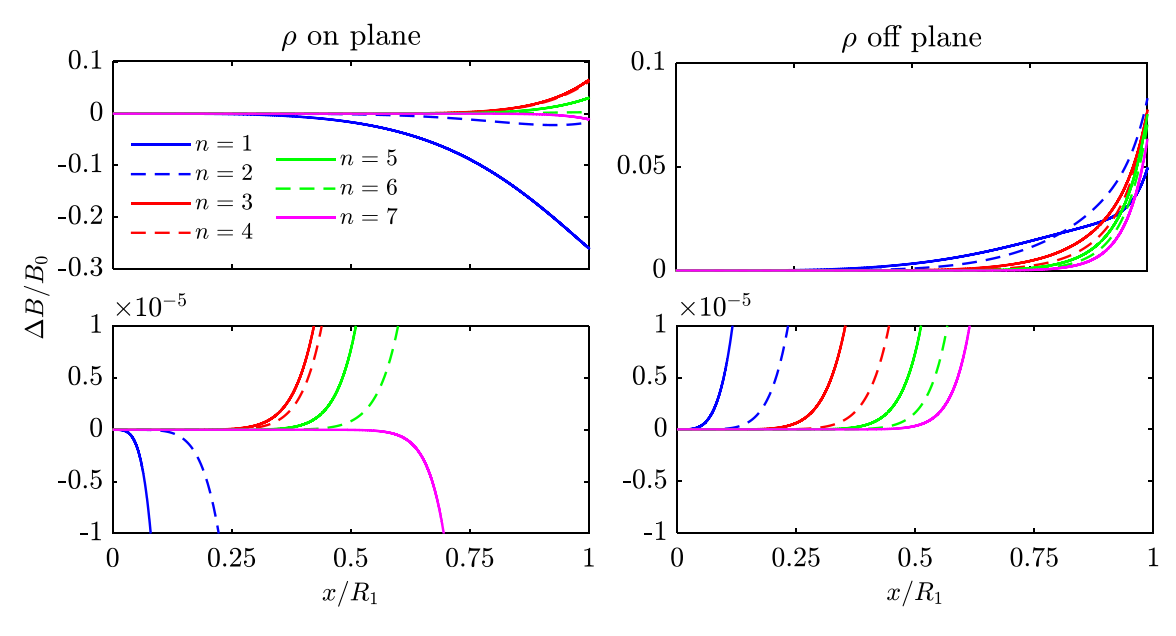


Fig. 12. The accuracy of the McDonald model along path  $\rho$  on and  $\rho$  off. The lower plots display the same data as the upper plots, but there has been zoomed in on the  $\Delta B/B_0$  axis.

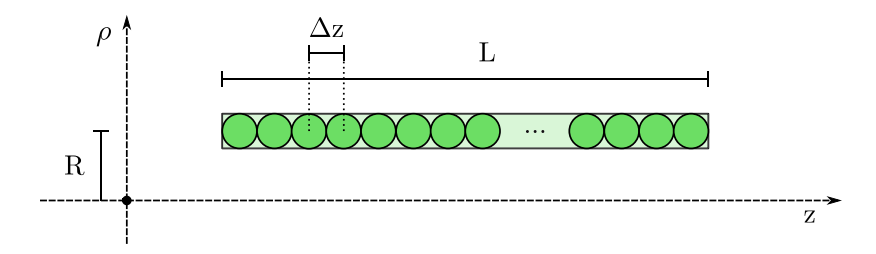


Fig. 13. A cross-sectional view of one side of the shell solenoid in the  $\rho z$ -plane. The figure indicates the length L, the radius R and the current loop separation  $\Delta z$ . The individual current loops are illustrated by the green circles. Notice that the perimeter of the current loops coincides with the left and right edge of the shell.

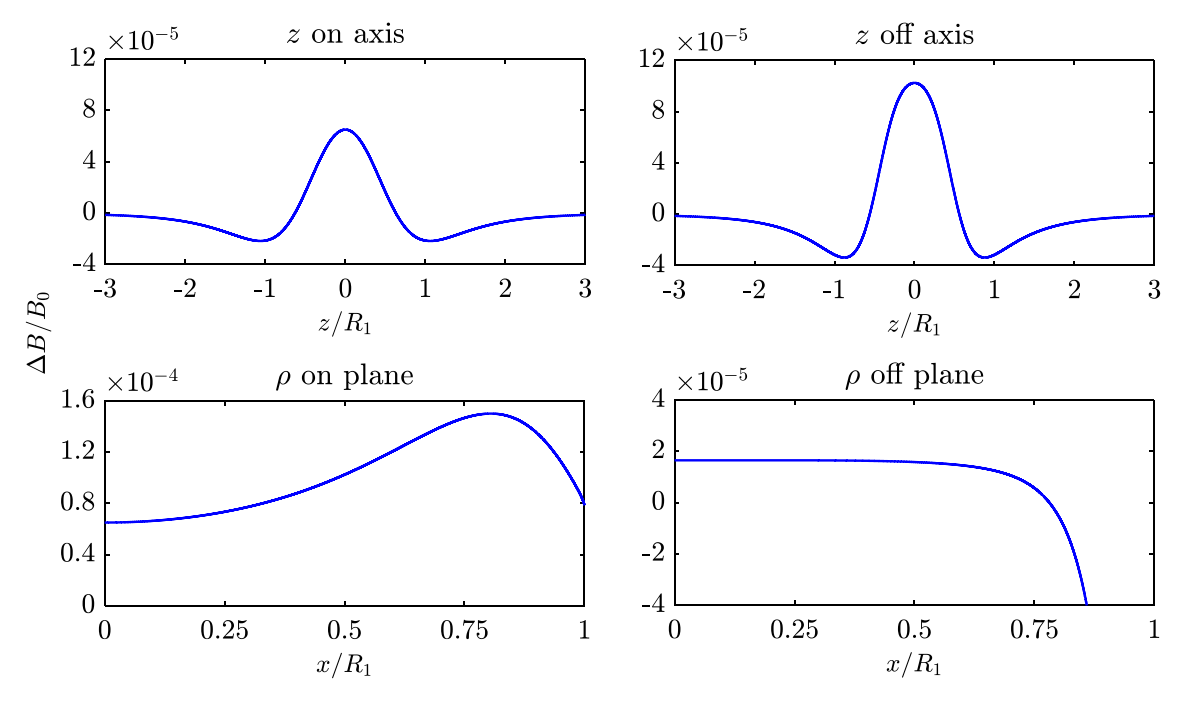


Fig. 14. The accuracy of the N-Wire model for a shell consisting of 30 circular current loops compared to the Conway model along the four paths.

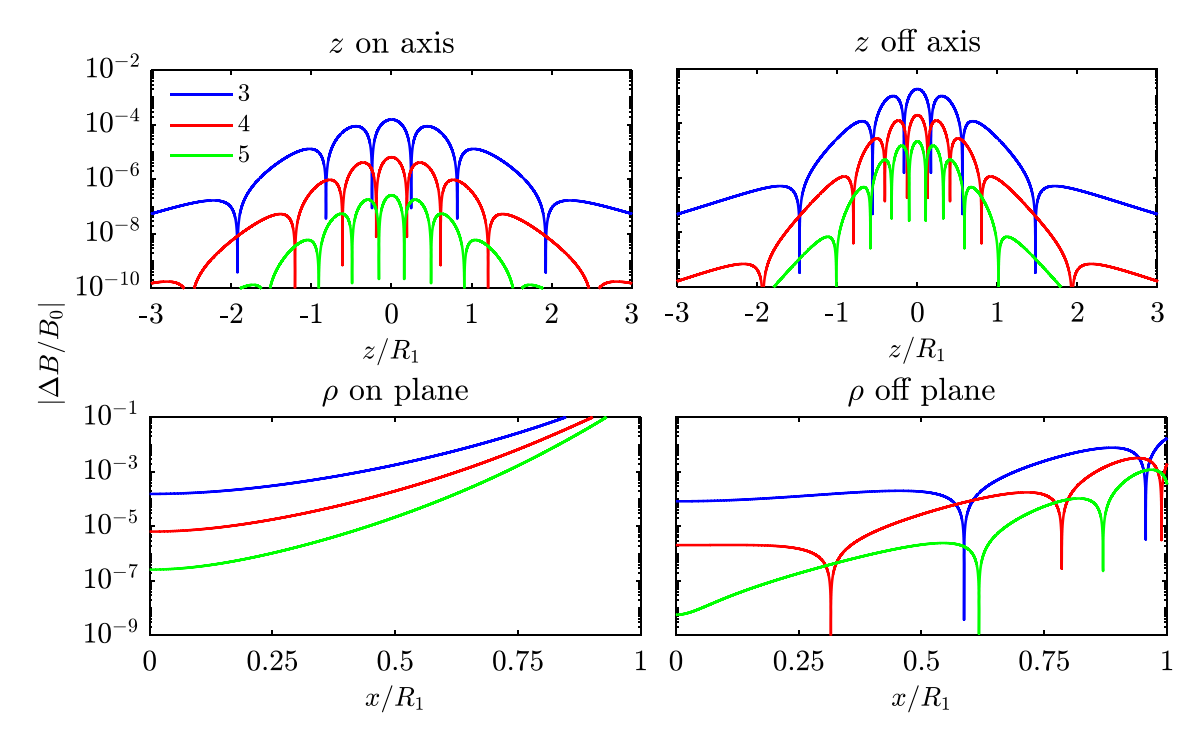
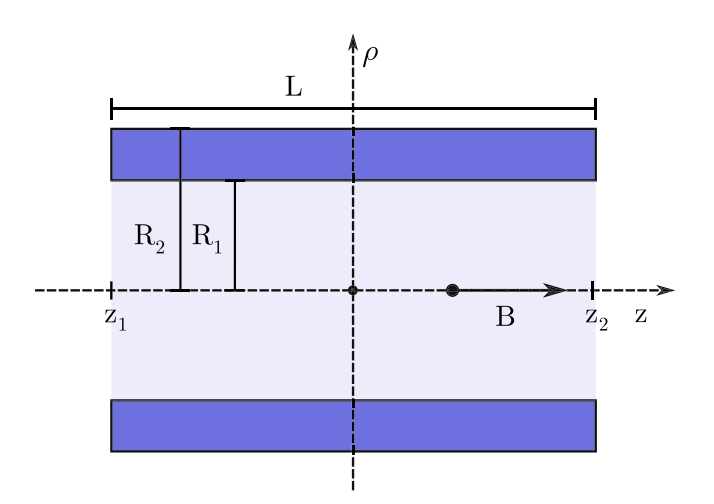


Fig. 15. The accuracy of the field calculated using the Gaussian quadrature method for 3, 4, and 5 loops. The Conway model has been used as a reference.



**Fig. 16.** A sketch showing a cross section of the finite solenoid in a cylindrical coordinate system. The inner and outer radius of the finite solenoid are denoted by  $R_1$  and  $R_2$  respectively. The z position of the left and right ends are denoted by  $z_1$  and  $z_2$ , and the total length of the solenoid by L. The current produces an on-axis field pointing in the z-direction.

current distributed over a greater length than the length of the shell. The SAM model is used to calculate the field of the individual loops. The accuracy of the *N*-wire model compared to the Conway model along the four paths can be seen in Fig. 14. It is on the  $10^{-5}$  to  $10^{-4}$  level for  $\rho/R < 0.75$ , which is comparable to the 4th and 5th order McDonald model.

# 5.4. Gaussian quadrature with loops for a shell

One could imagine that the computation time of the N-Wire model described in Section 5.3 could be reduced significantly without a big impact on the accuracy, if the shell was represented by a fewer loops chosen in a clever way. The total field would then be given as a weighted sum of the fields of the individual loops. Which loops give the

biggest contribution to the field at a certain position will depend on the point of evaluation, but a there exists algorithms to determine the overall best positions and weights of the loops. Gaussian quadrature as described in Abramowitz and Stegun [17] is such an algorithm. Representing a shell with a number of current loops, is equivalent to distributing point along a line. Using Legendre polynomials as the orthogonal basis, the positions and weights become the ones listed in [17, p. 921]. The resulting fields for a single shell represented by 3, 4, and 5 loop respectively can be seen in Fig. 15. The accuracy of the models is comparable to the some of the higher order McDonald models presented.

#### 5.5. Discussion of shell models

The computation times for the models examined are listed in Table 3, and are determined as described in chapter 3. For the thin shell solenoid the McDonald approximation is seen to be 1-2 orders of magnitude faster than the analytic Conway model. The accuracy of the McDonald model is below  $10^{-5}$  for some of the higher order models and  $\rho/R < 0.5$ . The Gaussian quadrature method is also seen to be faster than the Conway model, but it is about an order of magnitude slower than the McDonald model, even though they have comparable accuracy. The computation time of the N-Wire model is 7.8 µs, which corresponds to roughly 30 times that of the SAM model as expected. Hence, the N-Wire model is slower than all the other models. Of the different approximations the McDonald model seems to be the best choice in terms of both accuracy and speed.

# 6. Finite solenoids

A finite solenoid is defined as a current distribution consisting of a uniform current density running azimuthally around in a hollow cylinder. A sketch of the cross section of a finite solenoid can be seen in Fig. 16. This is similar to the shell described in chapter 5 but with a finite thickness. The on-axis field of the finite solenoid can be found by integrating equation (19) over a range of thin shell solenoids with varying radius. The resulting on-axis field of a finite solenoid is given by

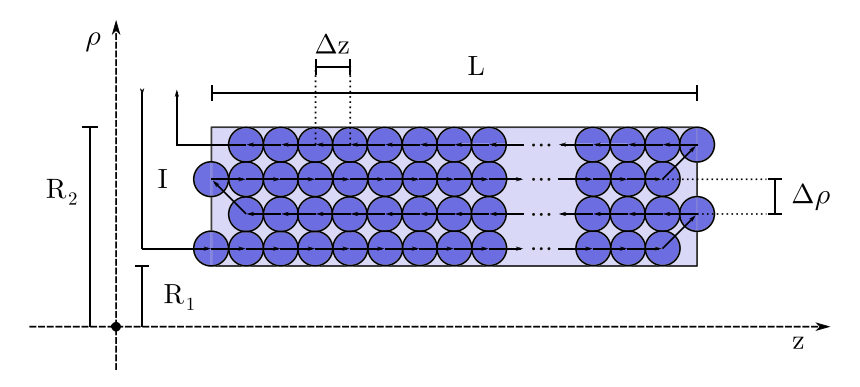


Fig. 17. A cross-sectional view of one side of half of the magnet model at the azimuthal angle  $\phi=0$  in the  $\rho z$ -plane. The figure indicates the length L, the inner radius  $R_1$ , the outer radius  $R_2$  and the winding separation in the  $\rho$  and z direction denoted  $\Delta \rho$  and  $\Delta z$  respectively. The individual wires in the model are represented by the blue circles. The arrows between the wires indicate how the coil is wound.

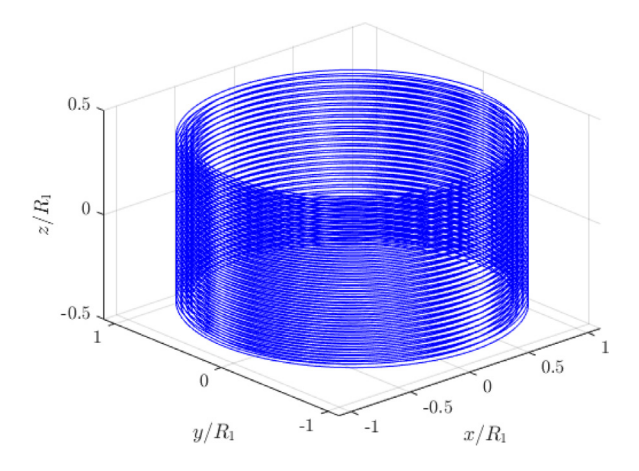


Fig. 18. A three-dimensional plot of the wire configuration of the Biot-Savart model

Table 3

The computation times determined as described in chapter 3 for calculating the magnetic field of a thin shell solenoid for the different models.

Model	Time [μs]
Conway	2.0
McD shell $n = 1$	0.049
McD shell $n = 2$	0.062
McD shell $n = 3$	0.074
McD shell $n = 4$	0.086
McD shell $n = 5$	0.093
McD shell $n = 6$	0.097
McD shell $n = 7$	0.12
N-Wire 1 × 30	7.8
GQ loops $n = 3$	0.82
GQ loops $n = 4$	1.1
GQ loops $n = 5$	1.3

$$B_{z} = \frac{\mu_{0}IN}{2L(R_{2} - R_{1})} \left[ (z - z_{1}) \ln \left( \frac{\sqrt{R_{2}^{2} + (z - z_{1})^{2}} + R_{2}}{\sqrt{R_{1}^{2} + (z - z_{1})^{2}} + R_{1}} \right) - (z - z_{2}) \ln \left( \frac{\sqrt{R_{2}^{2} + (z - z_{2})^{2}} + R_{2}}{\sqrt{R_{1}^{2} + (z - z_{2})^{2}} + R_{1}} \right) \right]$$
(32)

where  $R_1$  is the inner radius and  $R_2$  is the outer radius of the solenoid, L is the length, I is the current in the wire, and N is the number of wire turns. As in the previous chapters, this allows for an off-axis expansion of the magnetic field. Using an exact analytic expression to calculate the field at any point in space for a finite solenoid involves numeric

integration, which only makes the result as "exact" as the integration method. The previous chapters have focused on comparing models of ideal current distributions, but what matters from an experimental point of view is how well the models describe the field of a physical coil. For the finite solenoid, we have therefore chosen to compare the models to a Biot–Savart model with multiple layers of helical wires. This model is intended to reflect how the windings are positioned in the actual magnet.

# 6.1. Biot-Savart model of a solenoid

The Biot-Savart model is based on the actual wire configurations of the magnet described in chapter 1. The magnet is made up of four layers of wires, each consisting of 30 windings. A sketch of how the wires are wound can be seen in Fig. 17. Notice how the axial direction of the winding alternates between each consecutive layer to cancel out the azimuthal and radial components of the field. The wires in Fig. 17 have been illustrated as having some finite radius, but the model assumes the wires have no thickness3. The figure illustrates where the wires are placed in relation to the continuous current distribution presented in Fig. 16. The first layer is positioned at  $\rho = R_1 + \frac{\Delta \rho}{2}$ , so the edge of the wires in the inner and outer most layer coincides with the edge of the continuous current distribution. However, in the axial direction the centre of the first wire of each layer coincides with the edge of the continuous current distribution. In this way the mean axial position of a single winding is placed  $\frac{\Delta z}{2}$  from the edge of the continuous current distribution, similar to the radial direction.

The Biot–Savart model is made up of small straight wire segments, where the endpoint of the nth line-segment is increased in the  $\phi$ - and the z-coordinate relative to the (n-1)th segment. The length of the solenoid is L and the inner radius and outer radius are given by  $R_1$  and  $R_2$  respectively. The radial coordinate  $\rho$  stays the same for all segments in a given layer. In our model we have used  $N_{\rm BS}=1000$  segments per winding. As described in chapter 1, the number of wires per layer is  $N_{\rm W}=30$  and the number of layers  $N_{\rm L}=4$ . Hence, the total number of straight wire segments is given by  $N_{\rm BS}\times N_{\rm W}\times N_{\rm L}=120000$ . A three-dimensional plot of the wire model used for the Biot–Savart model can be seen in Fig. 18.

Compared to a physical magnet, some simplifications have been made in the magnet model. Firstly, the current leads carrying the current to and from the magnet have been excluded. Experimentally, these often introduce complications as they can generate a significant contribution to the magnetic field. Secondly, the different layers are not connected at the end turns. Instead, each layer consists of its own wire. The size of the magnetic field of the Biot–Savart model as well

<sup>&</sup>lt;sup>3</sup> Note that the thickness of the wires is a parameter that could be examined, but that is outside the scope of this paper.

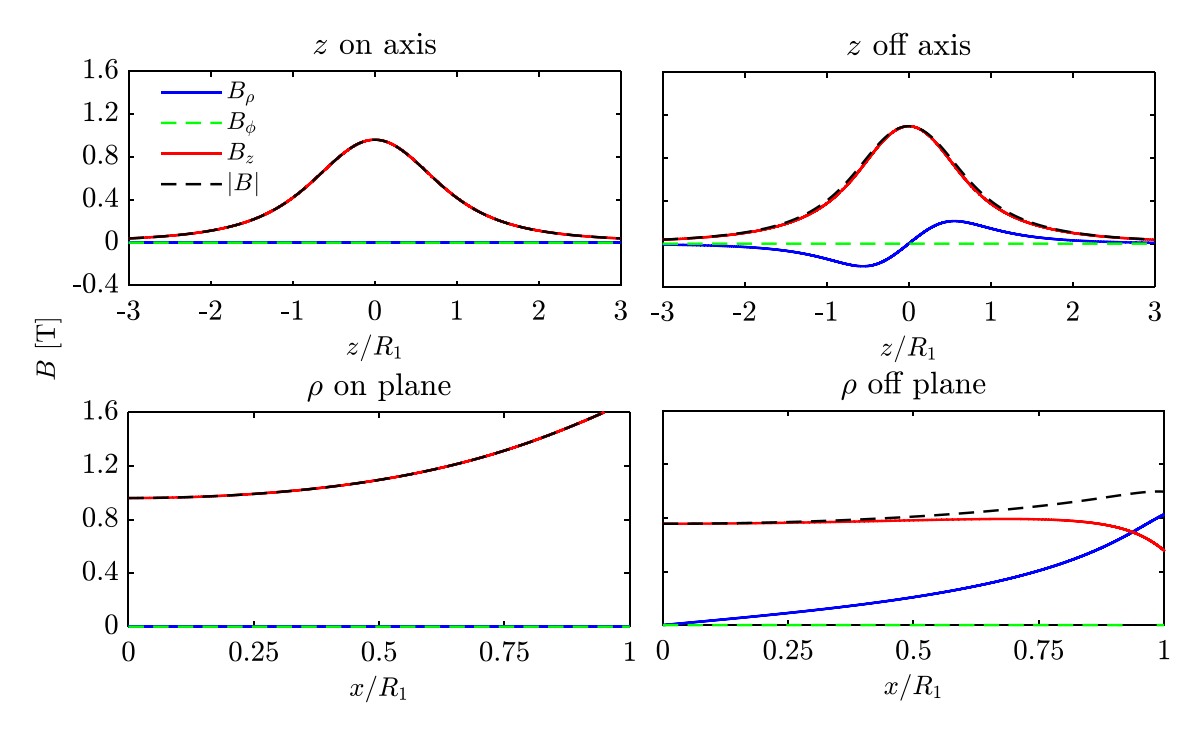


Fig. 19. The magnitude of magnetic field and its components as calculated by the Biot-Savart model along all four paths.

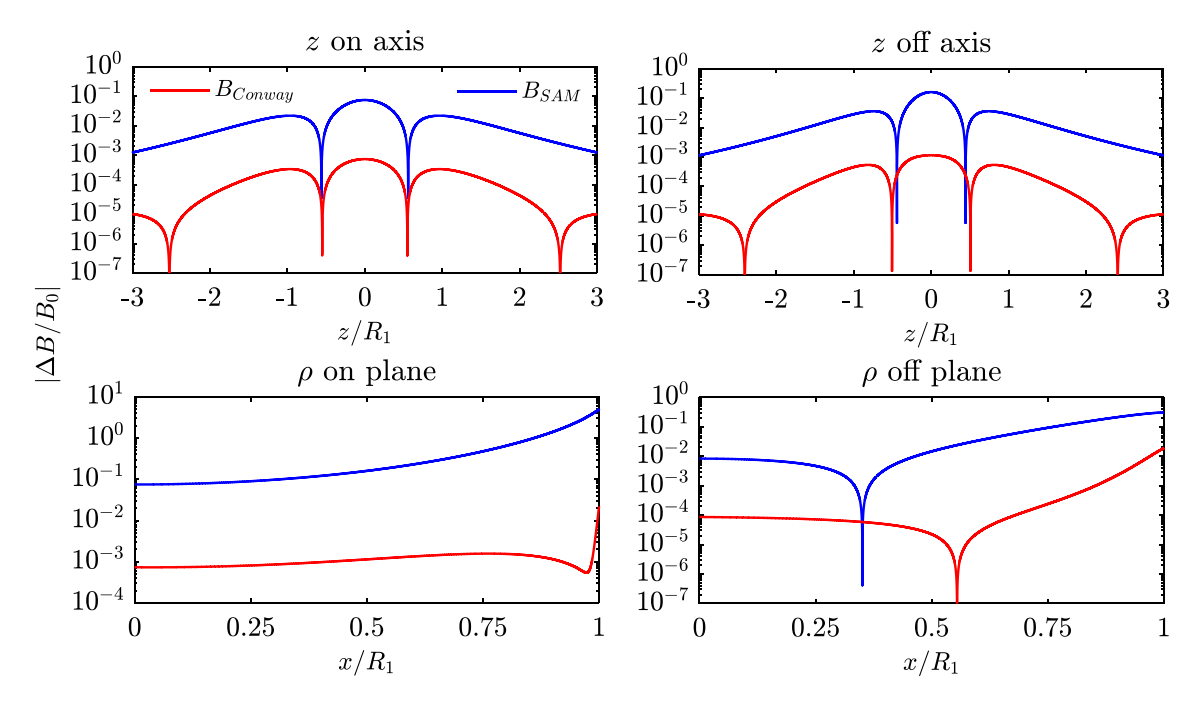


Fig. 20. The accuracy of the exact analytic expressions for a loop and a shell compared to a finite solenoid. The Biot-Savart model of a solenoid has been used as a reference model.

as the components along the four paths can be seen in Fig. 19. To give an idea the significance of a detailed solenoid model compared to a simple current loop or a shell, Fig. 20 shows a crude comparison between the three. For this plot, is has been assumed that the radius that is normalised to for the loop and shell models, is the same as the radius normalised to for the finite solenoid — that is  $R \approx R_1$ .

# 6.2. Truncated approximate vector potential model

The Truncated Approximate Vector Potential (TAVP) model, inspired by the Jackson model (see Section 4.4), has been used in simulations related to the ALPHA experiment [18, Appendix A.1]. The vector potential for a solenoid with radius R in spherical coordinates

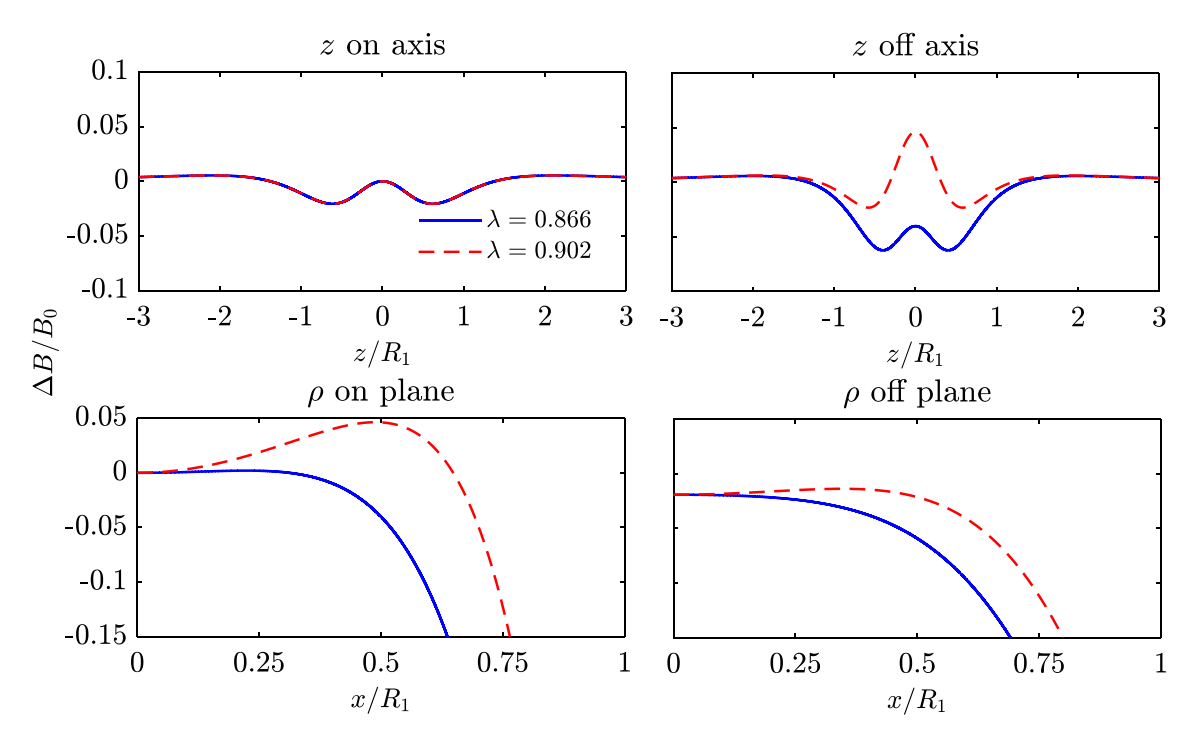


Fig. 21. The accuracy of the TAVP model along all four paths for different values of \(\delta\). The Biot-Savart model of a solenoid has been used as a reference model.

 $(r, \phi, \theta)$  is given as

$$A_{\phi} = \frac{C}{2R\lambda} \left( (R^2 + r^2 - 2R\lambda\rho)^{-1/2} - (R^2 + r^2 + 2R\lambda\rho)^{-1/2} \right), \tag{33}$$

where  $C=\frac{\mu_0IR^2}{4}$  is a constant, and  $\lambda$  is a parameter to be fitted to the exact field. For  $\lambda=0.866$  the first and the second terms of Eqs. (14) and (15) are reproduced, and  $\lambda=0.902$  corresponds to the best fit of the magnetic field of the mirrors [18]. The magnet modelled in [18] is the same as the magnet modelled in this paper. The radius inserted in the TAVP model is chosen so  $\Delta B(0,0,0)/B_0=0$ , which is fulfilled by  $R\approx 1.015R_2$ . The accuracy of the resulting field is plotted in Fig. 21. The TAVP model is seen to be orders of magnitude worse than the models previously examined.

# 6.3. McDonald model

Eq. (32) for the on-axis field can be used to make an off-axis expansion similar to what was done in Section 4.2. For the finite solenoid the model has been tested with up to 6 terms (n = 5). The accuracy of the McDonald model is seen in Figs. 22 and 23. Below each plot is a zoomed-in version.

# 6.3.1. Expanding the McDonald model

In this study, the McDonald model was initially calculated by hand to fifth order, but one could achieve any desired accuracy (within machine precision) by continuing expansion. Deriving the required derivatives could be very time consuming, but this paper presents an algorithm that allows easy expansion to any order. Looking at the expression for the McDonald model (Eqs. (10)–(12)) it is seen that calculating the sign, the denominator, and the power of  $\rho/2$  is trivial, so the only challenge is to calculate the nth derivative of the axial field (Eq. (32)). By adopting the following notation

$$z_i' = z - z_i \tag{34}$$

$$P_{ij} = \sqrt{R_i^2 + z_i'^2} \tag{35}$$

$$Q_{ij} = \sqrt{R_j^2 + z_i'^2} + R_j \tag{36}$$

$$C = \frac{\mu_0 I N}{2L(R_2 - R_1)} \tag{37}$$

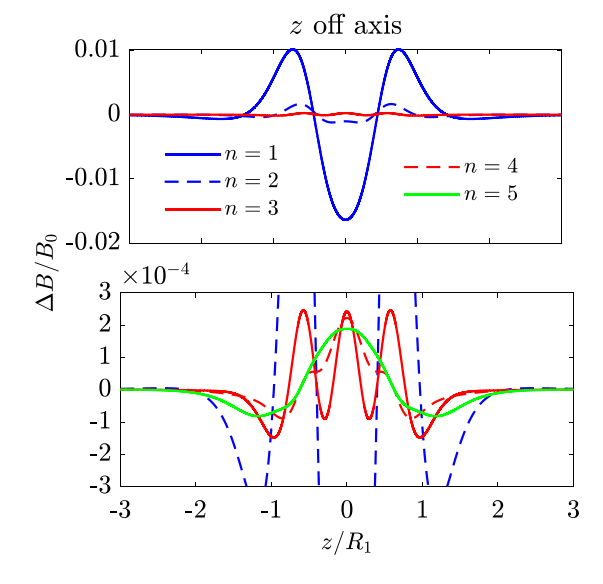


**Fig. 22.** The accuracy of the McDonald model along path z *off.* The upper plot displays the orders 1-4 while the lower plot is zoomed in on the  $\Delta B/B_0$  axis displays the orders 2-5. The Biot–Savart model of a solenoid has been used as a reference model.

where i, j = 1, 2 from Eq. (19), the on-axis field is given as

$$B_z(0,0,z) = C\left(z_1'\ln(Q_{12}) - z_1'\ln(Q_{11}) - z_2'\ln(Q_{22}) + z_2'\ln(Q_{21})\right) \tag{38}$$

$$= C \sum_{i,j} (-1)^{i=j} z_i' \ln(Q_{ij})$$
 (39)

This somewhat simpler expression is used to calculate  $a_0^{(n)}$ :

$$a_0^{(0)} = B_z(0, 0, z) (40)$$

$$a_0^{(1)} = C \sum_{i,j} (-1)^{i=j} \left( \ln(Q_{ij}) + \frac{z'^2}{P_{ij}Q_{ij}} \right)$$
 (41)

$$a_0^{(2)} = C \sum_{i,j} (-1)^{i-j} \left( 3 \frac{z'}{P_{ij}Q_{ij}} - \frac{z'^3}{P_{ij}^2 Q_{ij}^2} - \frac{z'^3}{P_{ij}^3 Q_{ij}} \right)$$
 (42)

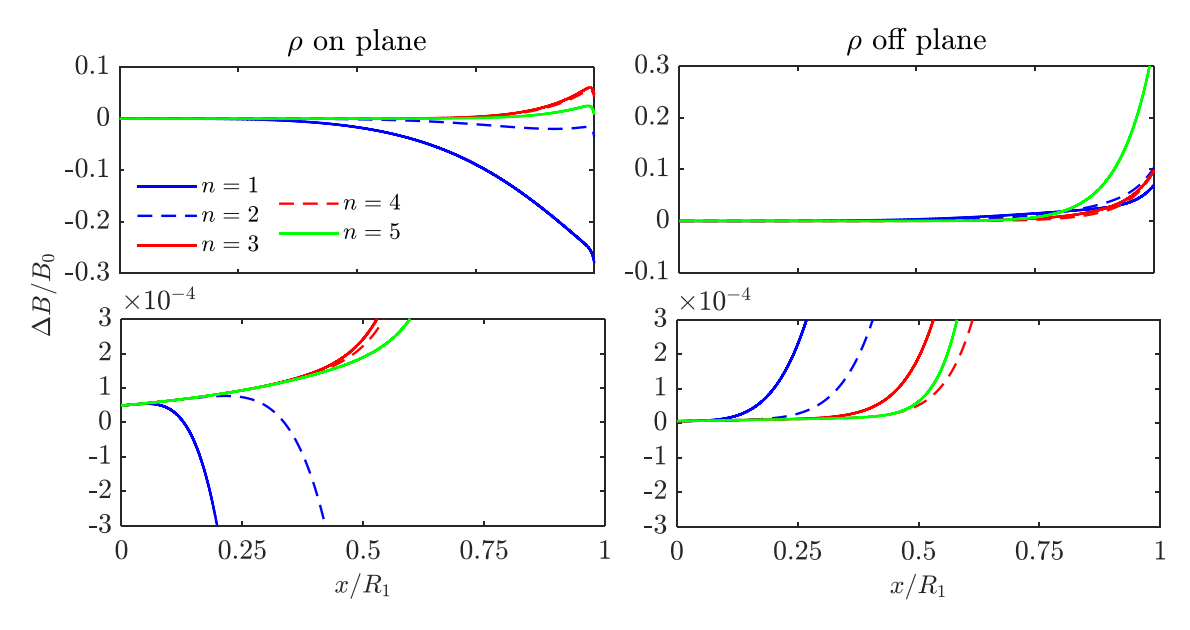


Fig. 23. The accuracy of the McDonald model along path  $\rho$  on and  $\rho$  off. The upper plot displays the same data as the lower plot, but the lower plot is zoomed in on the  $\Delta B/B_0$  axis. The Biot–Savart model of a solenoid has been used as a reference model.

Table 4
The number of (unique) terms  $N_T$  ( $N_T'$ ) as a function of the order of the expansion n.

,	1 1	
n	$N_T(n)$	$N_T'(n)$
0	4	4
1	8	8
2	12	12
3	36	24
4	108	36
5	324	56
6	972	72
7	2916	100

Thus  $a_0^{(2)}$  exclusively consists of terms of the form

$$k\frac{z'^{\lambda}}{P_{ij}^{\mu}Q_{ij}^{\nu}}\tag{43}$$

where  $\lambda, \mu, \nu \in \mathbb{N}$  and  $k \in \mathbb{Z}$ . The derivative is

$$\frac{d}{dz}\left(k\frac{z'^{\lambda}}{P_{ij}^{\mu}Q_{ij}^{\nu}}\right) = k\lambda\frac{z'^{(\lambda-1)}}{P_{ij}^{\mu}Q_{ij}^{\nu}} - k\nu\frac{z'^{(\lambda+1)}}{P_{ij}^{(\mu+1)}Q_{ij}^{(\nu+1)}} - k\mu\frac{z'^{(\lambda+1)}}{P_{ij}^{(\mu+2)}Q_{ij}^{\nu}}$$
(44)

The resulting three terms are also of the type given by Eq. (43). Hence, for  $n \geq 2$  all  $a_0^{(n)}$  will be given as a sum over such terms. The number of terms in  $a_0^{(n)}$  is  $N_T(n) = 4 \cdot 3^{n-1}$ , but several of the terms can be combined, as they have the same values of  $\lambda, \mu, \nu$ , so the total number of terms is  $N_T'$ . In the code, we combine these programmatically to reduce computation time. Table 4 shows the number of terms as a function of n.

# 6.4. N-wire model of a finite solenoid

Similar to how a thin shell solenoid was modelled using a number of equidistant circular current loops along a line in the *N*-wire model in Section 5.3, a finite solenoid can be modelled as a number of current loops placed in a 2D grid as seen in Fig. 24. In accordance with the magnet described in chapter 1, four layers of wires each consisting with of 30 current loops are used. Notice that the perimeter of the current loops coincides with the edges of the box. The field of each loop is calculated with the SAM model (Section 4.1). The accuracy of the N-Wire model for a finite solenoid is seen in Fig. 25.

# 6.5. Gaussian quadrature with loops for a solenoid

In the same way as a shell could be represented by a few current loops distributed along a line according to the Gaussian quadrature model described in Section 5.4, a finite solenoid can be represented by a low number of loops in a rectangular grid. When assigning the positions and the weights of the wires, the axial and radial dimensions are treated separately. As  $L\approx 10(R_2-R_1)$  for the magnet used as a model, it makes sense to have the number of loops in the axial dimension,  $N_z$ , bigger than the number of loops in the radial dimension,  $N_\rho$ . The accuracy of the most promising of the tested models are presented in Fig. 26. The models are denoted  $N_\rho \times N_z$ .

#### 6.6. Gaussian quadrature with shells for a solenoid

Rather than representing a finite solenoid with current loops placed in a 2D grid, the finite solenoid can be represented with a number of thin shell solenoids of the type described in chapter 5. Using the Gaussian quadrature method (as described in Section 5.4) to calculate the positions and weights of the shells, we show the resulting field in Fig. 27. The accuracy does not increase much for more than two shells. As the magnet used as a model (see chapter 1) is about 10 times longer than it is thick and only consists of 4 layers, this is not surprising.

#### 6.7. Discussion of solenoid models

The computation times for the models examined are listed in Table 5, and are determined as described in chapter 3. A detailed Biot–Savart model was used as a reference model, and unsurprisingly this was extremely slow compared to the approximations. The Truncated Approximate Vector Potential model and the lowest order McDonald models are the fastest. The speed comes at the price of accuracy, which for the TAVP model is only on the percent level. In comparison, the McDonald model can be made about two orders of magnitude more accurate for x/R < 0.4, while being 3-5 times slower. For a similar accuracy both the Gaussian quadrature models based on loops and solenoids are seen to be about an order of magnitude slower than the McDonald model. The N-wire model is accurate to about the same level as the Gaussian quadrature models, but it is an order of magnitude slower.

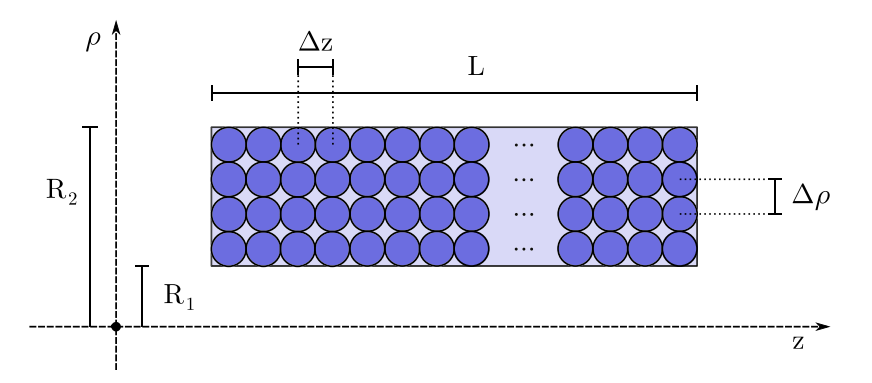


Fig. 24. A cross-sectional view of one side of the N-Wire model in the  $\rho z$ -plane. The figure indicates the length L, the inner radius  $R_1$ , the outer radius  $R_2$  and the current loop separation in  $\rho$  and z respectively denoted by  $\Delta \rho$  and  $\Delta z$ . The individual current loops are illustrated by the blue circles.

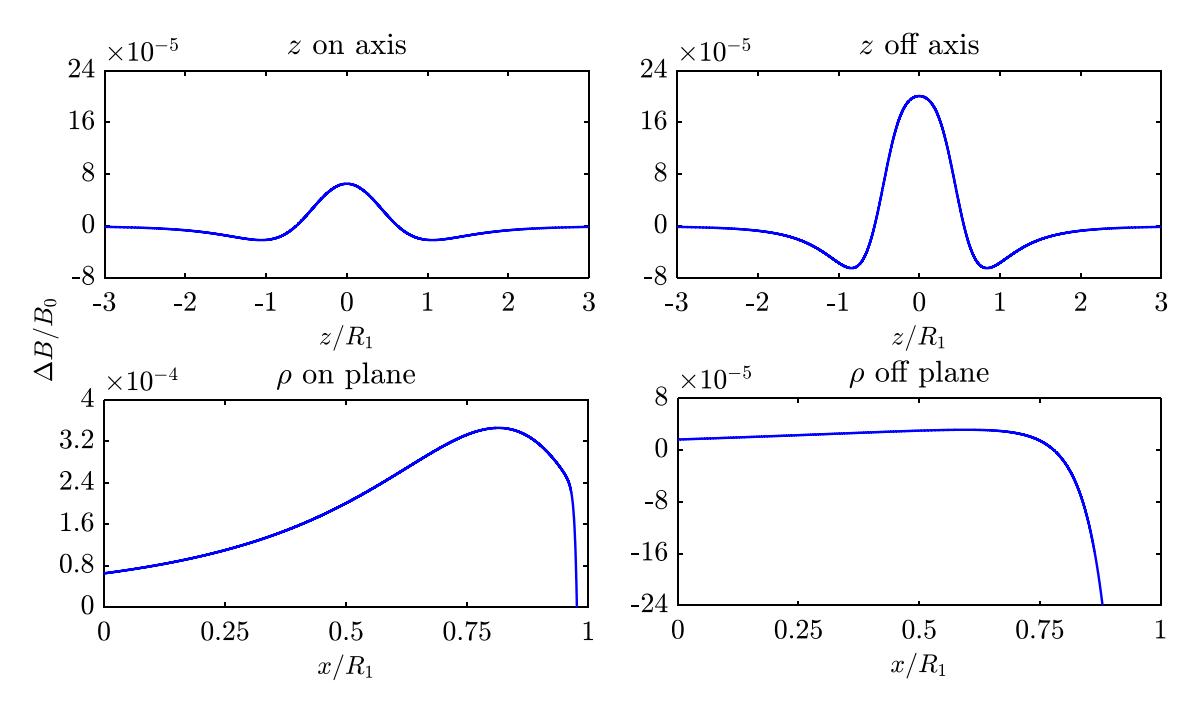


Fig. 25. The accuracy of the field calculated using the N-Wire model. The Biot-Savart model has been used as a reference.

**Table 5**The computation times determined as described in chapter 3 for calculating the magnetic field of a finite solenoid for the different models.

Model	Time [μs]
Biot-Savart	2300
TAVP	0.34
McD sol. $n = 1$	0.23
McD sol. $n = 2$	0.51
McD sol. $n = 3$	0.82
McD sol. $n = 4$	1.5
N-Wire $4 \times 30$	31
GQ loops $1 \times 3$	0.83
GQ loops 1 × 4	1.1
GQ loops 1 × 5	1.3
GQ loops 2 × 3	1.6
GQ shells $n = 1$	2.1
GQ shells $n = 2$	3.7
GQ shells $n = 3$	5.5
GQ shells $n = 4$	7.3

# 7. Conclusion

None of the examined models can unambiguously be said to be the best choice — it depends on the required accuracy and computation

time. However, the McDonald model excels in both speed and accuracy at low and high order respectively, and it is easy to adjust the order to one's needs. If time is not a concern a detailed Biot–Savart model will give the most accurate results, if analytic models are not an option.

The computation times of the thin shell models and the finite solenoid models are greater than the loop models by about a factor 2 and 10 respectively. At the same time, the importance for the accuracy of the more detailed magnet models has been illustrated by Fig. 20.

# CRediT authorship contribution statement

Peter Granum: Conceptualization, Methodology, Software, Formal analysis, Investigation, Writing – original draft, Writing – review & editing, Visualization, Supervision. Magnus Linnet Madsen: Software, Formal analysis, Investigation, Writing – original draft, Visualization. Joseph Tiarnan Kerr McKenna: Software, Investigation, Writing – original draft. Danielle Louise Hodgkinson: Conceptualization, Methodology, Software, Writing – review & editing. Joel Fajans: Conceptualization, Methodology, Writing – review & editing, Supervision.

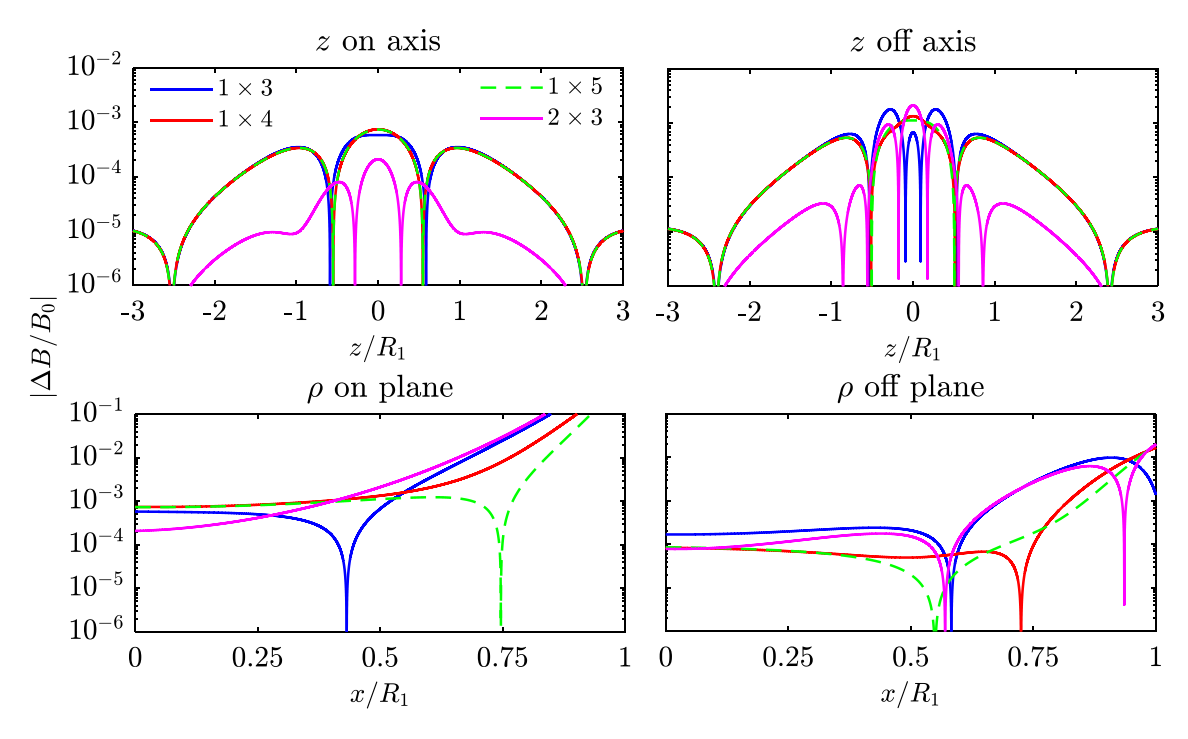


Fig. 26. The accuracy of the field calculated using the Gaussian quadrature method using multiple current loops in different configurations. The wire configuration used for each plot is denoted  $N_{\rho} \times N_{z}$ , where the first and second index denotes the number of loops in the radial and the axial direction respectively.

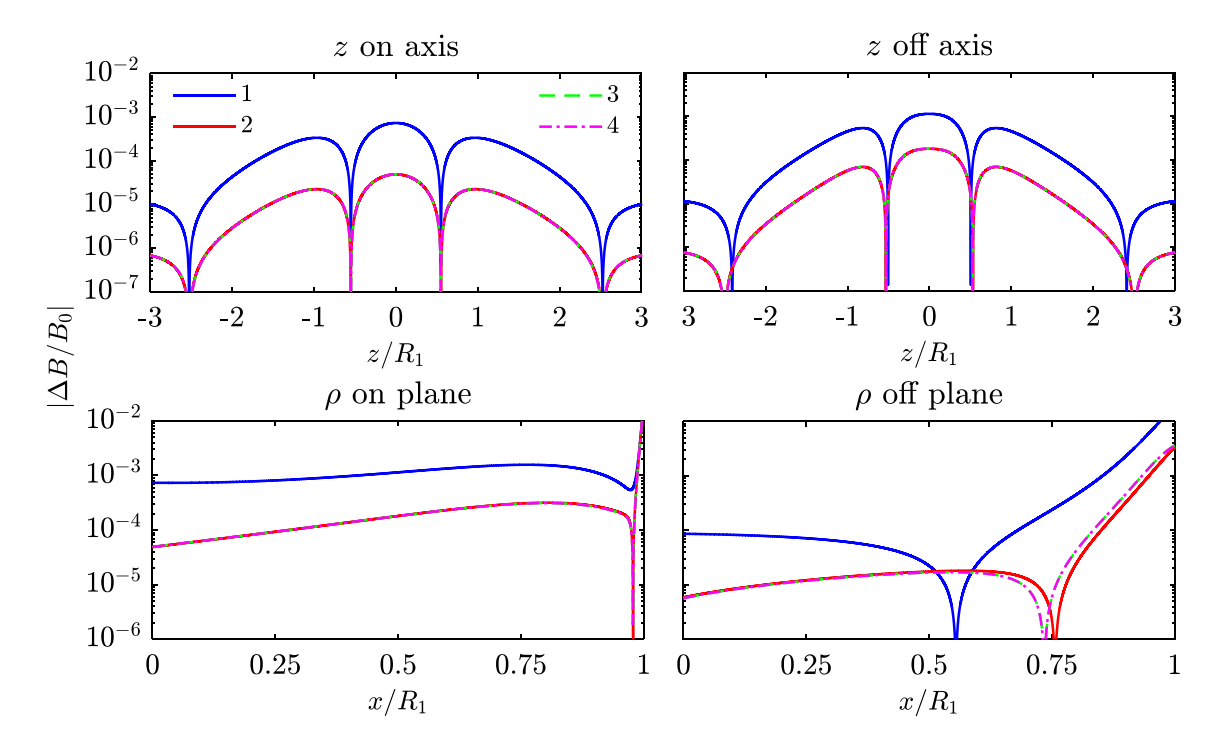


Fig. 27. The accuracy of the magnetic field calculated using the Gaussian quadrature method based on different numbers of shell solenoids. 1, 2, 3 and 4 shells have been used.

# Declaration of competing interest

# The authors declare that they have no known competing financial interests or personal relationships that could have appeared to influence the work reported in this paper.

# Data availability

The generated datasets are available from Peter Granum on reasonable request.

#### Acknowledgements

This work was supported by the Carlsberg Foundation (Denmark), EPSRC (UK), and DOE, NSF (USA). We are grateful to the CERN IT department for the computing services. Thanks to Karen Zukor for her help with the editing process.

#### References

- [1] G.B. Andresen, et al., Trapped antihydrogen, Nature 468 (2010) 673-676.
- [2] G.B. Andresen, et al., Confinement of antihydrogen for 1,000 seconds, Nat. Phys. 7 (7) (2011) 558–564.
- [3] C. Amole, et al., Resonant quantum transitions in trapped antihydrogen atoms, Nature 483 (7390) (2012) 439.
- [4] M. Ahmadi, et al., Observation of the 1S–2S transition in trapped antihydrogen, Nature 541 (7638) (2017) 506.
- [5] C. Amole, et al., Description and first application of a new technique to measure the gravitational mass of antihydrogen, Nature Commun. 4 (1) (2013).
- [6] C. Amole, et al., An experimental limit on the charge of antihydrogen, Nature Commun. 5 (1) (2014) 1.
- [7] M. Ahmadi, et al., An improved limit on the charge of antihydrogen from stochastic acceleration, Nature 529 (7586) (2016) 373.

- [8] M. Ahmadi, et al., Observation of the hyperfine spectrum of antihydrogen, Nature 548 (7665) (2017) 66.
- [9] M. Ahmadi, et al., Characterization of the 1S–2S transition in antihydrogen, Nature 557 (7703) (2018).
- [10] M. Ahmadi, et al., Observation of the 1S–2P Lyman-α transition in antihydrogen, Nature 561 (7722) (2018) 211.
- [11] E.D. Hunter, A. Christensen, J. Fajans, T. Friesen, E. Kur, J.S. Wurtele, Electron cyclotron resonance (ECR) magnetometry with a plasma reservoir, Phys. Plasmas 27 (3) (2020) 032106.
- [12] David J. Griffiths, Introduction to Electrodynamics, fourth ed., Pearson Cambridge University Press 2017, 2017.
- [13] J. Simpson, J. Lane, C. Immer, R. Yuongquist, Simple analytic expressions for the magnetic field of a circular current loop, 2001, Unpublished, https: //ntrs.nasa.gov/citations/20010038494 (Accessed 1 May 2021).
- [14] Kirk T. McDonald, Expansion of an axially symmetric, static magnetic field in terms of its axial field, 2015, URL https://physics.princeton.edu/~mcdonald/ examples/axial.pdf (Accessed 1 May 2021).
- [15] John David Jackson, Classical Electrodynamics, John Wiley & Sons Inc, 1998.
- [16] J.T. Conway, Exact solutions for the magnetic fields of axisymmetric solenoids and current distributions, IEEE Trans. Magn. 37 (4) (2001) 2977–2988.
- [17] Milton Abramowitz, Irene A. Stegun, Handbook of Mathematical Functions, with Formulas, Graphs, and Mathematical Tables, Dover Publications, Inc., USA, 1974.
- [18] C. Amole, et al., Discriminating between antihydrogen and mirror-trapped antiprotons in a minimum-b trap, New J. Phys. 14 (1) (2012) 015010.